

Fluorescence Lifetime Imaging Microscopy (FLIM) of Intracellular Transport by Means of Doubly Labelled siRNA Architectures

Larissa Doll,^[a] Jens Lackner,^[b] Franziska Rönicke,^[a] Gerd Ulrich Nienhaus,^[b, c, d, e] and Hans-Achim Wagenknecht*^[a]

For monitoring the intracellular pathway of small interfering RNA (siRNA), both strands were labelled at internal positions by two ATTO dyes as an interstrand Förster resonance energy transfer pair. siRNA double strands show red emission and a short donor lifetime as readout, whereas siRNA antisense single strands show green emission and a long donor lifetime. This readout signals if GFP silencing can be expected (green) or not (red). We attached both dyes to three structurally different alkyne anchors by postsynthetic modifications. There is only a

slight preference for the ribofuranoside anchors with the dyes at their 2'-positions. For the first time, the delivery and fate of siRNA in live HeLa cells was tracked by fluorescence lifetime imaging microscopy (FLIM), which revealed a clear relationship between intracellular transport using different transfection methods and knockdown of GFP expression, which demonstrates the potential of our siRNA architectures as a tool for future development of effective siRNA.

Introduction

Gene silencing by small interfering RNA (siRNA) provides an effective approach for mRNA degradation and results in a knockdown of the encoded protein.^[1] The development of siRNA therapeutics is still challenging, however, due to low RNA stability, insufficient delivery to target cells, ineffective endosomal escape and off-target effects.^[2] To overcome these drawbacks, it is of fundamental interest to devise ways to monitor the uptake of siRNA probes, their intracellular integrity and subsequent processing in living cells. To this end, fluorescence imaging is a suitable technique.^[3] The combination of two different fluorophores in complementary oligonucleotides, which only undergo Förster resonance energy transfer

(FRET) while in proximity to each other, makes fluorescence imaging even more powerful. Thus, it is possible to distinguish between double- and single-stranded siRNA simply by their fluorescence readout color.^[4] Surprisingly, only very few examples of such siRNA constructs have been published hitherto, and in most of these, the two fluorophores were attached to the termini of the siRNA strands.^[5] Helm et al.^[5b,d] used such architectures to study siRNA delivery and degradation inside living cells. Moreover, fluorescence lifetime imaging microscopy (FLIM) has not yet been used to study siRNA dynamics. For FRET analysis, one can benefit from its single channel readout, by just following the changes in the donor dye lifetime. In addition, FLIM-FRET is less sensitive to background and photobleaching effects than intensity-based fluorescence measurements. We previously reported the concept of "RNA traffic lights", which is an RNA architecture based on a two-color fluorescence readout (Figure 1).^[6] In contrast to the conventional terminal attachment of chromophores, we labelled RNA at internal positions of the sequence by an interstrand energy transfer pair responding better to dehybridization of the RNA duplex.^[6a] Besides incorporation of the dyes as base surrogates,^[6a] we were able to attach the dyes post-synthetically via copper-catalyzed azide-alkyne cycloaddition (CuAAC) to different alkyne moieties, including 2'-propargylated ribo- and arabinofuranosides and acyclic aminopropanediol linkers. This makes the RNA constructs synthetically more accessible and enables the use of a variety of chromophores.^[6b,d,7] The photostability of this fluorescent siRNA architecture was further improved by combinations of our photostable cyanine-styryl-dyes.^[8] These fluorophores, however, show multiple fluorescence lifetimes due to different interactions with RNA, making FLIM-FRET experiments impossible.^[6d] For this purpose, we transferred the "RNA traffic light" concept (Figure 1) to photostable ATTO dyes. We present herein the development of fluorescent siRNA architectures that


[a] Dr. L. Doll, Dr. F. Rönicke, Prof. Dr. H.-A. Wagenknecht
Karlsruhe Institute of Technology (KIT), Institute of Organic Chemistry
Fritz-Haber-Weg 6, 76131 Karlsruhe (Germany)
E-mail: Wagenknecht@kit.edu


[b] J. Lackner, Prof. Dr. G. U. Nienhaus
Karlsruhe Institute of Technology (KIT), Institute of Applied Physics
Wolfgang-Gaede-Str. 1, 76131 Karlsruhe (Germany)

[c] Prof. Dr. G. U. Nienhaus
Institute of Nanotechnology (INT), Karlsruhe Institute of Technology (KIT)
76344 Eggenstein-Leopoldshafen (Germany)

[d] Prof. Dr. G. U. Nienhaus
Institute of Biological and Chemical Systems (IBCS)
Karlsruhe Institute of Technology (KIT)
76344 Eggenstein-Leopoldshafen (Germany)

[e] Prof. Dr. G. U. Nienhaus
Department of Physics, University of Illinois at Urbana-Champaign
1110 West Green Street, Urbana, IL 61801 (USA)

 Supporting information for this article is available on the WWW under <https://doi.org/10.1002/cbic.202100150>

 © 2021 The Authors. ChemBioChem published by Wiley-VCH GmbH. This is an open access article under the terms of the Creative Commons Attribution Non-Commercial License, which permits use, distribution and reproduction in any medium, provided the original work is properly cited and is not used for commercial purposes.

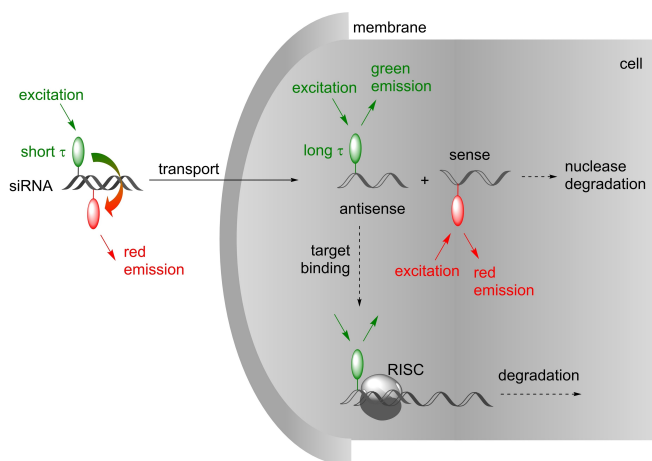


Figure 1. Concept of “siRNA traffic lights”: RNA is labelled at internal positions of the sequence by two different fluorescent dyes that undergo interstrand energy transfer. Dehybridization of the siRNA can be imaged by a red-to-green fluorescence color transition, as well as a change in the fluorescence lifetime (τ) of the donor dye (green). The subsequent steps, general nuclease degradation, mRNA target binding and mRNA degradation in the RISC complex are not addressed in this work.

are labelled with two different ATTO dyes as FRET pair. For the first time, the delivery and fate of siRNA in living cells was tracked in real time by FLIM.

Results and Discussion

Design, synthesis and optical characterization of the FRET-based siRNA architecture

The siRNA architectures based on the eGFP mRNA sequence were labelled at internal positions by an interstrand FRET pair. The antisense oligonucleotide was modified with the donor fluorophore (Do) ATTO532 and the sense strand with the acceptor fluorophore (Ac) ATTO647 N (Figure 2). The siRNA double strands show red fluorescence (635–800 nm) by the ATTO647 N dye when the ATTO532 dye is excited at 532 nm. The emission is shifted to green (542–635 nm), however, after processing of siRNA into single stranded antisense RNA, potentially binding to target mRNA. We first studied a structurally diverse approach by different dye anchors. This is important, because we incorporated both dyes very close to each other (below the Förster radius) outside the seed region of the siRNA architecture to avoid potential interference with the recognition sequence of the RISC complex in the seed region and to maintain its binding specificity to mRNA. Three structurally different alkyne building blocks were used as nucleotide anchors (Figure 2): (i) the 2'-propargylated uridine (cU in RNA1–RNA2) with the natural-like ribo-configuration, (ii) the acyclic and alkynylated (S)-2-amino-1,3-propanediol linker (cL in RNA3–RNA4), and (iii) the 2'-propargylated uridine analogue with arabino configuration (cAraU in RNA5–RNA6). In all three cases, the postsynthetic strategy to modify the siRNA strands with the dyes by copper(I)-catalyzed alkyne-azide cyclo-

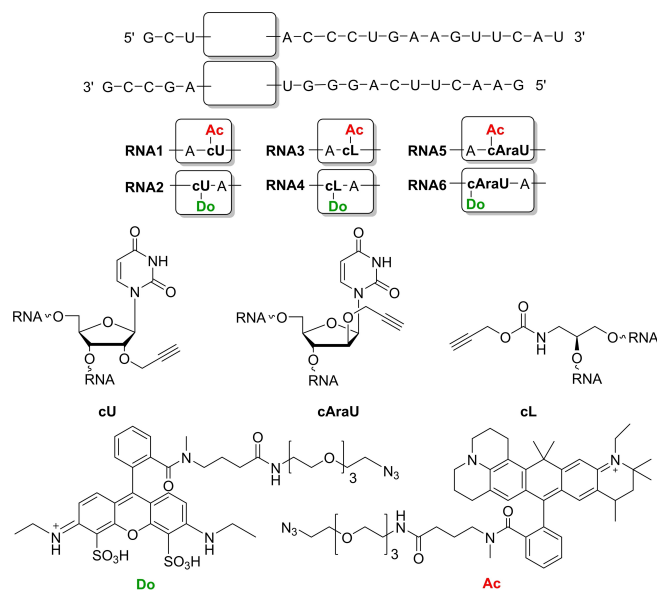


Figure 2. Sequences of RNA1–RNA6 for basic studies by optical spectroscopy and structures of alkyne-bearing click moieties cU, cAraU, cL as well as of ATTO532 (Do) and ATTO647N (Ac).

addition allows a facile synthetic access to the new RNA library, without the time-consuming route via dye phosphoramidites as RNA building blocks. The extended structural diversity increases the chances for selecting the siRNA architecture with the best energy transfer efficiency.

To study the impact of the fluorophore anchors on the RNA double helix stabilities as well as their energy transfer efficiencies, we characterized the optical properties of the different structural variations in RNA1–RNA6 in buffer solution (10 mM Na-P_i, 250 mM NaCl, pH 7). The distinct spectral separation of the absorption maxima at 532 nm (Do) and 647 nm (Ac) (Figure S16) shows that these fluorophores can be excited independently and do not form dimers by excitonic interactions. Additionally, the ATTO dyes exhibit higher extinction coefficients than our former cyanine-styryl dyes, leading to an increased fluorescence brightness. The different chromophore anchors do not significantly affect the fluorescence readout, which can probably be attributed to the long, flexible and soluble PEG-linkers between the RNA and the ATTO dyes. The fluorescence color contrast ratios (measured with 532 nm excitation) range from $I_{Ac}/I_{Do}=2.7$ for RNA1–RNA2, $I_{Ac}/I_{Do}=2.4$ for RNA3–RNA4 to $I_{Ac}/I_{Do}=2.1$ for RNA5–RNA6 (Table S3). Taken together, the siRNA double strand RNA1–RNA2 allows better fluorescence imaging although its fluorescence ratio is lower than those of the previously published siRNA architectures with cyanine-styryl dyes ($I_{Ac}/I_{Do}=4.5$ for a sequence similar to RNA1–RNA2), as it shows only a single fluorescence lifetime and not multiple ones due to different dye-RNA interactions. The melting temperature T_m was highest for RNA1–RNA2, $T_m=84^\circ\text{C}$ and revealed a destabilizing effect of the dye modifications in RNA2–RNA3 ($T_m=77^\circ\text{C}$) and RNA3–RNA4 ($T_m=77^\circ\text{C}$).

Since there was no significant difference in fluorescence readout between the different anchors cL, cU and cAraU, and

the duplex stability was highest in **RNA1-RNA2**, we only used the commercially available anchor **cU** and focused on improving the two-color readout (Figure 3). We synthesized the terminally labelled **RNA7-RNA8** because conventional siRNA constructs are modified at the 3'-end of the antisense strand. **RNA7-RNA8** does not exhibit a better energy transfer readout ($I_{Ac}/I_{Do}=2.6$), which results from a lower acceptor extinction. Furthermore, we placed an additional intervening **A-U**-pair between the dyes in **RNA9-RNA10**. The resulting emission spectrum (Figure 4) as well as the contrast ratio of $I_{Ac}/I_{Do}=3.2$ shows that the enlarged distance has a positive impact on the energy transfer and demonstrates that our interstrand siRNA-FRET architectures can be tuned and optimized in contrast to the conventional, terminally labelled siRNA constructs. Both duplexes have similar melting temperatures ($T_m=84^\circ\text{C}$ for **RNA7-RNA8** and 81°C for **RNA9-RNA10**).

Based on these results, we applied the concept to the target mRNA sequence **eGFP** such that inhibition of the gene silencing mechanism by a miRNA-like pathway is avoided.^[9] Accordingly, we capped both 3'-ends in **RNA11-RNA12** with a two-uridine-overhang to enhance stability inside the cell as well as improve recruitment into an RNA-induced silencing complex (RISC).^[10] Since we replaced two uridines as dye anchors in the **eGFP** sequence by the "clickable" artificial building block **cU**, the FRET

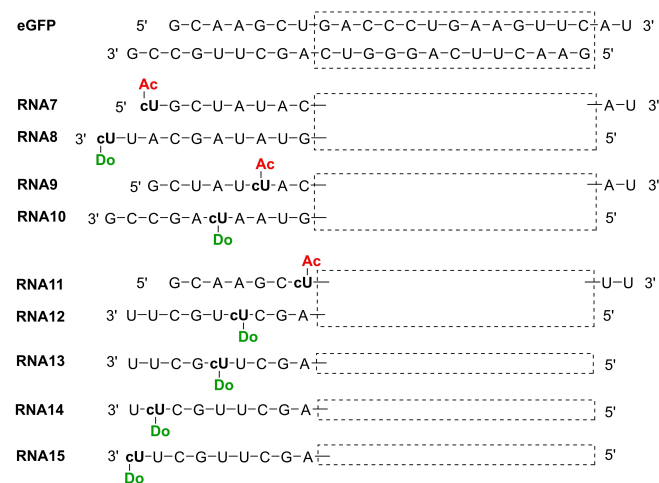


Figure 3. Sequences of **RNA7-RNA15**, which are fully complementary to **eGFP** mRNA. For structures of **cU**, **Do** and **Ac**, see Figure 2.

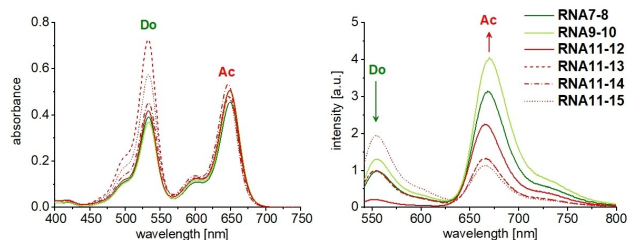


Figure 4. UV/Vis absorbance (left) and steady-state fluorescence (right) of double-stranded siRNA architectures (for sequences see Figure 3), $2.5\ \mu\text{M}$ in $10\ \text{mM Na-P}_i$ buffer, $250\ \text{mM NaCl}$, $\text{pH } 7$, 20°C , $\lambda_{\text{exc}}=532\ \text{nm}$.

pair is now separated by two intervening base pairs. Additionally, we tried siRNA architectures with a larger distance between donor and acceptor dye (**RNA11-RNA13/-RNA14/-RNA15**). The change of the 3'-overhang from **C-G** to **U-U** has the additional advantage that there is no **G-C** pair placed next to the dyes in **RNA11-14** and **RNA11-15** that might quench the emission^[11] and, consequently, might have a negative impact on the energy transfer. Indeed, steady-state fluorescence as well as quantum yield measurements show a distinct reduction in fluorescence intensity not only for the FRET pairs but also for the single strands. **RNA11-RNA12** shows a high contrast ratio $I_{Ac}/I_{Do}=10.6$ and a nearly completely quenched green fluorescence ($\Phi_F=0.02$) due to a very efficient energy transfer (Table 1). The apparent energy transfer efficiency E_{app} which can be determined as the ratio of acceptor intensity to the total fluorescence intensity of donor and acceptor, equals 91%. The stability is remarkably high ($T_m=85^\circ\text{C}$). Further enhanced distances of up to seven intervening base pairs or nucleotides, respectively, in the overhang between the dyes in **RNA11-RNA13**, **RNA11-RNA14** and **RNA11-RNA15** did not lead to improved fluorescence readout properties. Thus, **RNA11-RNA12** is the best candidate for imaging of intracellular siRNA transport by steady-state confocal microscopy and FLIM.

Steady-state cell imaging and GFP knockdown experiments

After identification of the optimal siRNA architecture for FRET, we visualized the siRNA uptake into cells and analyzed the impact of the attached dyes to the gene silencing function by performing GFP knockdown experiments. Firstly, human cervix carcinoma (HeLa) cells were transfected with $10\ \text{pmol RNA11-RNA12}$ as well as **RNA11ds** (i.e., **RNA11** annealed with the unmodified counterstrand, no **Do** dye) and **RNA12ds** (i.e., **RNA12** annealed with the unmodified counterstrand, no **Ac** dye) as controls without the acceptor dye modification using *ScreenFect*[®] as the transfection reagent (Figures 5 and S19). After incubation for 24 h, transfected samples were visualized by live-cell confocal fluorescence microscopy. The **Do** dye of the FRET pair was excited with a laser at $532\ \text{nm}$ and the

Table 1. Fluorescence color contrasts I_{Ac}/I_{Do} , apparent energy transfer efficiency E_{app} , fluorescence lifetimes τ and quantum yields Φ_F of the double strands **RNA9-RNA10** and **RNA11-RNA12** as well as their respective single strands.

RNA	I_{Ac}/I_{Do} ^[a]	E_{app} ^[a,b]	Φ_F Do ^[c]	τ Do (ns)	Φ_F Ac ^[d]
RNA9	–	–	–	–	0.51
RNA10	–	–	0.64	–	–
RNA9-RNA10	3.2	0.76	0.05	n.d.	0.19
RNA11	–	–	–	–	0.46 ^[f]
RNA11ds ^[e]	–	–	–	–	0.52
RNA12	–	–	0.49 ^[f]	3.5 ± 0.2	–
RNA12ds ^[e]	–	–	0.69	3.7 ± 0.2	–
RNA11-RNA12	10.6	0.91	0.02	0.2 ± 0.2	0.19 ^[f]

[a] $\lambda_{\text{exc}}=532\ \text{nm}$. [b] $E_{\text{app}}=I_{Ac}/(I_{Ac}+I_{Do})$. [c] $\lambda_{\text{exc}}=532\ \text{nm}$, $\lambda_{\text{em}}=542-657\ \text{nm}$. [d] $\lambda_{\text{exc}}=647\ \text{nm}$, $\lambda_{\text{em}}=657-800\ \text{nm}$. [e] annealed with unmodified counterstrand. [f] See Figure S18.

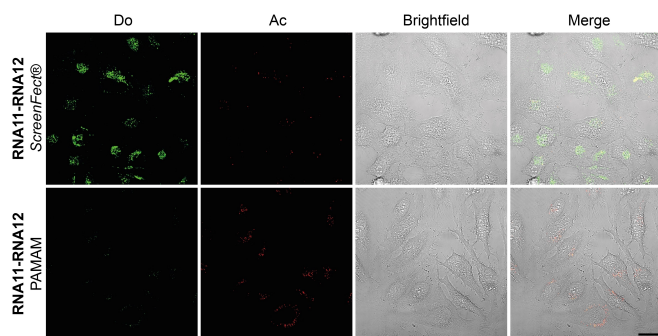


Figure 5. Confocal laser scanning images 24 h after transfection of HeLa cells with 50 pmol **RNA11-RNA12** by means of *ScreenFect*[®] and PAMAM dendrimer. $\lambda_{\text{exc}} = 532$ nm, $\lambda_{\text{em}} = 542\text{--}572$ nm (**Do**) and $\lambda_{\text{em}} = 657\text{--}687$ nm (**Ac**). Scale bar: 25 μm .

emission was separately detected in two different channels at 550–600 nm (for the green **Do** signal) and 665–705 nm (for the red **Ac** signal). Against our expectations, we observed only a strong green fluorescence signal, indicating a dehybridized siRNA inside the cell (Figure 5). This dehybridization might be a response of the siRNA to the pH change caused by the *ScreenFect*[®] solution, which was added to the sample before transfection and visible after mixing it with the DMEM medium, which contains the pH indicator phenol red. The pH-dependent fluorescence measurements (Figure S17) confirmed a shutdown of FRET at lower pH value due to dehybridization. According to our imaging results, *ScreenFect*[®] dehybridized siRNA double strands and primarily transports siRNA single strands into cells. As alternative to *ScreenFect*[®], we used a polyamidoamine dendrimer (PAMAM, generation 5) with a triethanolamine core, which is known to efficiently deliver siRNA by forming electrostatic complexes.^[12] Transfection of 50 pmol **RNA11-RNA12** was performed in serum free medium for 8 h to prevent electrostatic interactions with serum proteins. Afterwards, the medium was exchanged and the cells were imaged after a total cell incubation time of 24 h. Then, a clear FRET signal with a strong red emission of the acceptor dye, compared to the relatively weak green signal of the donor dye, was visible (Figure 5). This microscopy result is consistent with the previously measured high FRET efficiency in **RNA11-RNA12** and proves that this dendrimer transports siRNA double strands into cells.

To rule out that the biological activity of **RNA11-RNA12** is affected by the dye modifications at internal positions of the RNA sequence, we transfected a HeLa/GFP cell line with our siRNA architecture and *Silencer*[®] GFP siRNA as a positive control for comparison (Figure 6). Again, we used both transfection methods. After incubation for 48 h, cells transfected with **RNA11-RNA12** and *ScreenFect*[®] showed a significant decrease of the GFP signal compared to the positive control, whereas the reduction of the GFP emission was less pronounced for cells transfected with **RNA11-RNA12** and PAMAM. Additional control experiments with the double-stranded eGFP siRNA (equivalent to **RNA11-RNA12** without any dye modifications, see Figure 3) also proved the knockdown and support our observation that the internal dye modifications do not influence the siRNA

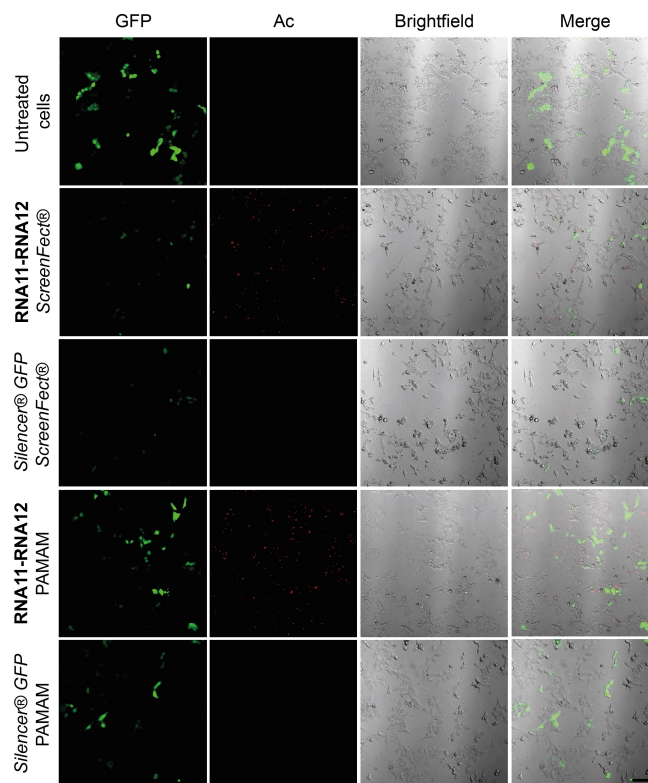


Figure 6. GFP knockdown imaged by confocal microscopy: HeLa/GFP cells were transfected with 10 pmol siRNA (**RNA11-RNA12** and *Silencer*[®] GFP) using *ScreenFect*[®] or PAMAM dendrimer for 48 h. GFP: $\lambda_{\text{exc}} = 488$ nm and $\lambda_{\text{em}} = 495\text{--}545$ nm, **Ac**: $\lambda_{\text{exc}} = 532$ nm and $\lambda_{\text{em}} = 657\text{--}687$ nm. Scale bar: 100 μm .

activity (Figure S20). These observations track well with the imaging data in HeLa cells. With *ScreenFect*[®], we mainly saw the green fluorescence of the biologically active antisense strand **RNA12**, still with the potential to induce gene silencing. In contrast, with the PAMAM dendrimer, we saw mainly red fluorescence attributed to the not yet dehybridized double strand **RNA11-RNA12**, which did not undergo the process of RNA-induced gene silencing yet. These results show nicely that our siRNA architecture not only maintains its biological knockdown function despite the dye modifications outside of the seed region of the siRNA sequence (as defined above), but elucidates also its potential for imaging of intracellular transport.

Fluorescence lifetime-based measurements

For deeper insight into the intracellular transport, as well as the processing of the siRNA, we used FLIM-FRET as a quantitative method. With our “siRNA traffic lights”, it should be possible to follow the changes in the hybridization states of the siRNA (siRNA double strands, single stranded antisense RNA and antisense RNA bound to the mRNA) in a single channel experiment, by just tracking the changes in the lifetime of the green donor dye (ATTO532). To test the applicability of our

siRNA system for FLIM, we firstly measured fluorescence lifetimes of the green donor dye in the FRET pair **RNA11-RNA12**, the single strand **RNA12** after dissociation as well as its hybrid **RNA12ds** with an unmodified counterstrand by using time-correlated single photon counting (TCSPC). The decay curves (Figure S21) of **RNA12** and **RNA12ds** can be fitted with a mono-exponential decay function. In agreement with the quantum yields, the fluorescence lifetime of the donor single strand, $\tau = (3.5 \pm 0.2)$ ns, is slightly shorter than the one of the single-labelled double strand, $\tau = (3.7 \pm 0.2)$ ns (Table 1). Both lifetimes can be assigned to the unquenched donor dye. In contrast, the fluorescence decay of the doubly modified siRNA **RNA11-RNA12** cannot be fitted by a single exponential but requires a biexponential decay function. This results in a 92% contribution of a short lifetime, $\tau_1 = (0.2 \pm 0.2)$ ns, whereas the remaining portion of 8% is attributed to a long fluorescence lifetime, $\tau_2 = (3.4 \pm 0.2)$ ns. This result suggests that the long lifetime can be assigned to a fraction of dehybridized antisense strands (see above).

Although the lifetimes of **RNA12** and **RNA12ds** are too close to separate them via FLIM, it should be possible to distinguish the quenched donor dye in siRNA **RNA11-RNA12** from unquenched antisense strands inside living cells. For the experiment, HeLa cells were transfected with **RNA11-RNA12** using either *XFect*[®] (Figure 7A–C, Figure S23) or PAMAM dendrimer (Figure S24). We used *XFect*[®] because we observed, as described above, that *ScreenFect*[®] dissociates the siRNA duplexes *before* their transport into the cells, so no further fluorescence lifetime change would be observable (Figure S22). The different behavior when using the two transfection

reagents is also seen in the fluorescence lifetimes of the green donor dye in the FRET pair **RNA11-RNA12** (Figure S22).

FLIM images were obtained every 15 min (*XFect*[®]) or 30 min (PAMAM dendrimer) over a period of 3 h (*XFect*[®]) or 4 h (PAMAM dendrimer), directly after starting the transfection. In the images, the color code was assigned to the corresponding emission color readout of the siRNA architecture: short fluorescence lifetimes are depicted in red, indicating energy transfer (with **Ac** in the counterstrand and red emission as readout), whereas long lifetimes are shown in green and are assigned to **Do** single strands (and green emission as readout). The FLIM-FRET experiments show broad distributions of lifetimes in the cell regions, which is illustrated by the histograms compiled from the 0 min and 150 min snapshots of HeLa cells transfected with **RNA11-RNA12** and *XFect*[®] (Figure 7B). The histogram of the first image (0 min) already shows a significant population with average lifetimes longer than 1 ns, which is not expected from the in-vitro experiments. Apparently, a considerable fraction of **RNA11-RNA12** is already dehybridized at the earliest times within single pixels of the FLIM image, presumably due to the presence of *XFect*[®] (Figure S22) and other interactions with the cell sample. Nevertheless, populations with shorter (≤ 2.7 ns, red) and longer (≥ 3.3 ns, green) average lifetimes can be well separated, corresponding predominantly to double-stranded siRNA and unquenched antisense strands, respectively. Using *XFect*[®] as transfection agent (Figure 7A, Figure S23), polyplexes with short lifetimes were observed near the cell membrane. After uptake of the probes into the cells, there was an increase in fluorescence lifetime, followed by an accumulation around the nucleus. This behavior was retarded by using PAMAM dendrimer as transfection reagent (Figure S24). After a total acquisition time of 4 h, only a few signals with long lifetime and almost no accumulation persisted, which fits well to the GFP knockdown experiments. The differences in the behavior, using either *XFect*[®] or the PAMAM dendrimer, can be quantified by tracking the changes of the fluorescence lifetimes within the cell regions. Therefore, the summed-up decay curves in three cell regions were fitted globally with a biexponential decay function with fixed lifetimes of 0.7 ns and 3.5 ns. The changes of the ratio of the amplitudes $A(3.5 \text{ ns})/A(0.7 \text{ ns})$ over time (Figure 7C, Figure S24) show that the long lifetime component is predominant in the course of the experiment when using *XFect*[®]. For the PAMAM dendrimer, in contrast, significant changes are absent.

These results indicate that **RNA11-RNA12** is processed in the cells using *XFect*[®], resulting in the expected increase of the fluorescence lifetime of the conjugated ATTO532 donor dye. With the PAMAM dendrimer, **RNA11-RNA12** is not processed, most likely due to an insufficient release from the dendrimer after cellular uptake. Although Figures 7 and S24 show data from only three cells, we performed three and four independent experiments with the dendrimer and *XFect* transfection reagents, respectively, all showing qualitatively the same behavior.

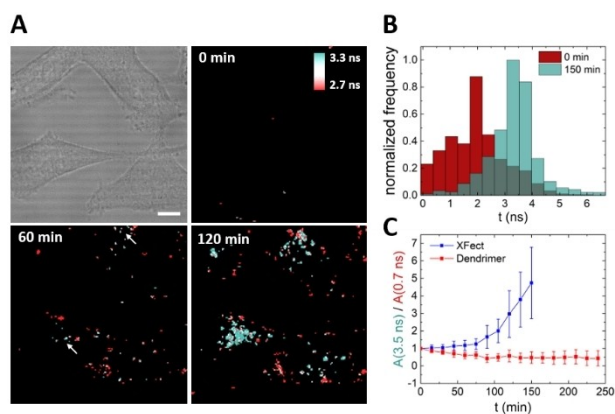


Figure 7. FLIM measurements. (A) Bright field image and FLIM images of HeLa cells transfected with **RNA11-RNA12** using *XFect*[®]. Short lifetimes (≤ 2.7 ns) are indicated in red, long lifetimes (≥ 3.3 ns) in green. White arrows show regions where long lifetime signals start to accumulate after 60 min. Scale bar 10 μm . (B) Lifetime histograms depicting distributions of fluorescence lifetimes at the beginning (0 min) and the end (150 min) of the FLIM measurement. The histograms are normalized by the total photon counts. (C) Time dependence of the ratio of amplitudes (long lifetime/short lifetime) of the fluorescence decay curves (integrated over selected regions) of three cells. The amplitudes were determined by a global fit with lifetimes fixed to 0.7 and 3.5 ns. Data for transfection with *XFect*[®] (A, B) and PAMAM dendrimer are shown in blue and red, respectively. Error bars indicate the standard deviation between the cell regions. All data points have been normalized to the value of 1 at 0 min.

Conclusion

In our siRNA architectures, the two RNA single strands were labelled at internal positions of the eGFP sequence by an ATTO dye pair that is coupled by interstrand FRET. Annealed siRNA double strands show the red emission of the acceptor dye and short lifetime of the donor dye due to FRET, whereas dehybridized siRNA antisense single strands show the green emission and long lifetimes of the donor single strands. Thus, the fluorescence readout of siRNA architectures can be considered as “traffic lights” that show if gene silencing can be expected (green) or not (red). We attached these dyes post-synthetically via copper-catalyzed azide-alkyne cycloaddition (CuAAC) to alkyne moieties in structurally different nucleotide anchors, including 2'-propargylated ribo- and arabinofuranosides and an acyclic aminopropanediol linker. This postsynthetic approach makes the siRNA architectures synthetically accessible in short time. The type of nucleotide anchoring does not significantly influence the energy transfer and thereby the fluorescence readout; there is only a slight preference by the fluorescence properties for the natural-like ribofuranoside anchor with the dye attached to the 2'-position. For the first time, the delivery and fate of siRNA in living cells was tracked not only by conventional confocal microscopy but additionally by FLIM. Our “siRNA traffic lights” permitted tracking of siRNA delivery and the investigation of siRNA mediated gene silencing using GFP-expressing HeLa cells. The FLIM experiments revealed a better transfection of HeLa cells and a better release of the antisense siRNA strands by the *ScreenFect*[®] and *XFect*[®] agents, resulting in a GFP knockdown, whereas the PAMAM dendrimer only transports double stranded siRNA into cells, which barely dehybridize and only poorly knock down GFP expression. These results demonstrate the power of doubly labelled siRNA architectures for the precise FLIM method.

Experimental Section

RNA synthesis: Oligonucleotides were prepared with a H-6 Synthesizer from K&A using standard phosphoramidite chemistry. Reagents and CPG columns (1 μmol) were purchased from Sigma Aldrich, Glen Research, Chem Genes and SAFC Prologo Reagents. The synthesis of cL^[13] and cAraU^[14] were reported elsewhere. All alkyne-modified RNA oligonucleotides were synthesized with an extended coupling time of 10 min. After preparation, the oligonucleotides were cleaved from the resin and deprotected on-bead by treatment with 1 mL of a 1:1 solution of conc. NH₄OH/methylamine for 20 min at room temperature and afterwards transferred into Eppendorf tubes and heated for 10 min at 65 °C. The oligonucleotides were dried and clicked with the respective dye 1 or 2 (see below). The TBDMS protecting group was removed by using a solution of DMSO and Et₃N-HF at 65 °C for 2 h. The modified RNA was precipitated with trimethyl(propoxy)silane and diethylether overnight at -32 °C. After washing with diethylether, the pellet was dried and then purified via HPLC as described in Supporting Information (Table S2). After MALDI mass spectrometry (Table S1, Figures S1–S15), pure fractions were collected, dried and quantified by their absorbance in water at 260 nm, using a NanoDrop ND-100 spectrophotometer. Duplexes were formed by heating to 90 °C for 10 min followed by slow cooling.

Click reaction (CuAAC): To the lyophilized alkyne-modified RNA water (100 μL), sodium ascorbate (25 μL of 0.4 M in water), dye azide (114 μL of 0.01 M in DMSO/ t-BuOH 3:1), a mixture of tris [(1-benzyl-1H-1,2,3-triazol-4-yl)methyl]amine (34 μL of 0.1 M in DMSO/t-BuOH 3:1), and tetrakis(acetonitrile) copper(I) hexafluorophosphate (17 μL of 0.1 M in DMSO/t-BuOH 3:1) were added. The reaction mixture was kept at 60 °C for 1.5 h. After cooling to room temperature, RNA was precipitated by adding Na₂EDTA (200 μL of 0.05 M in water), sodium acetate (450 μL of 0.3 M in water) and ethanol (10 mL, 100%) and stored at -32 °C overnight. After centrifugation, the supernatant was removed and the residue washed two times with cold ethanol (2 mL, 80%).

Spectroscopic measurements: Optical characterization was performed in NaP_i buffer solution (10 mM) using quartz glass cuvettes (10 mm) (2.5 μM DNA and 250 mM NaCl). Absorption spectra were recorded with a Varian Cary 100 spectrometer, fluorescence was measured with a Jobin-Yvon Fluoromax 3 fluorimeter with a slit width of 2 nm. All spectra are corrected for Raman emission from the buffer solution.

Cell experiments and confocal fluorescence microscopy: Human cervix carcinoma cells (HeLa cells) or HeLa/GFP cells (AKR-213) were cultured in Dulbecco's modified Eagle medium (DMEM) supplemented with 10% fetal bovine serum and 1% penicillin/streptomycin at 37 °C in a 5% CO₂ atmosphere. 24 h before transfection 8 × 10⁴ HeLa cells per well were seeded in an 8-well chamber slide (μSlide 8 well ibiTreat, IBIDI, Martinsried, Germany) in 200 μL of media. For transfection, 10 pmol/50 pmol of the RNA duplexes were diluted in *ScreenFect*[®] dilution buffer (Incella, Eggenstein-Leopoldshafen, Germany) to a final volume of 10 μL. 10 μL of a 1:10 dilution of *ScreenFect*[®] siRNA in dilution buffer were added to the diluted RNA and rapidly mixed. A subsequent incubation time of 30 min at room temperature allowed the formation of lipoplexes (liposome-RNA complexes). The transfection mixture was then added to the cells. The cells were incubated for 24 h/48 h with the respective transfection mixture at 37 °C in a 5% CO₂ atmosphere. The visualization of the probes was performed by confocal laser scanning microscopy using a Leica TCS SPE (DMI8) inverted microscope with an ACS APO 63×/1.30 oil or an ACS APO 10×/0.30 DRY objective. The donor (Do) was excited at 532 nm and the acceptor (Ac) at 635 nm. The emission was detected in spectral windows of 542–572 nm (green) and 657–687 nm (red). GFP was excited at 488 nm and emission detected at 495–545 nm. Using the acquisition software Leica Application Suite (LAS) X 2.0.1.14392, the picture ratio was adjusted to 1024×1024 pixels 8 bit depth.

Gene silencing: HeLa/GFP cells (AKR-213) expressing enhanced green fluorescent protein (EGFP) were applied to measure the knockdown of siRNA. siRNA was delivered either in the form of polyplexes or lipoplexes. Polyplexes were fabricated with biodegradable poly(amidoamine), and lipoplexes were prepared using *ScreenFect*[®] GFP siRNA according to the manufacturer's protocol. *Silence*[®] GFP siRNA (Thermo Fisher Scientific) was used as a positive control. Lipoplexes were directly mixed with 8 × 10⁴ cells per well and seeded in an 8-well chamber slide (μSlide 8 well ibiTreat, IBIDI, Martinsried, Germany) whereas cells were grown for 24 h, first, and afterwards transfected with polyplexes in serum free medium. After 8 h, the medium was removed and replaced with fresh culture medium. After 48 h, cells were analyzed by confocal microscopy using an excitation wavelength of 488 nm and an emission bandpass filter at 495–545 nm.

Lifetime imaging setup: All fluorescence lifetime and FLIM measurements were carried out on a time-resolving confocal microscope system (MicroTime 200, PicoQuant, Berlin, Germany) described previously.^[15] Fluorescence was excited with light from a 532 nm picosecond-pulsed diode laser (LDH-P-FA-530, PicoQuant)

running at 26 MHz; the emission was collected through a bandpass filter (575/50 nm center/width, Chroma, Bellows Falls, VT, USA). Data were acquired and analyzed with SymPhoTime software (PicoQuant).

Lifetime measurements: Two borosilicate cover glass slides (25 × 40 mm² and 20 × 20 mm², VWR, Radnor, PA) were briefly torched over a flame to remove contaminants and glued together using two pieces of double-sided adhesive tape, leaving a 3 mm wide channel in the middle. The channel was filled with 20 μl of a 250 nM RNA solution (RNA12, RNA12ds or RNA11-RNA12). For acquisition of lifetime decays, data were taken for 2 min with 5 μW laser power. The instrument response function (IRF) was determined under the same conditions using Rose Bengal (Sigma-Aldrich, St. Louis, MO) as a reference. Fluorescence decay curves were analyzed using our own Matlab script (The MathWorks, Natick, MA). For fitting, the measured decay curves were convoluted with the IRF and fitted with an exponential or biexponential function for singly and doubly labeled RNA strands, respectively.

FLIM imaging: HeLa cells were seeded into an 8-well chamber (Lab-Tek borosilicate Chambered Coverglass, Thermo Fisher Scientific, Waltham, MA) with a confluency between 50 and 70%. On the following day, the cells were imaged for 2.5 h in steps of 15 min directly after exposing the cells to doubly labelled siRNA strands. To facilitate their uptake, Xfect[®] (Takara, Shiga, Japan) was used as transfection agent according to the manufacturer's protocol using 6.25 pmol siRNA. During the measurement, the 8-well chamber was placed into an environmental chamber (H301 Electric Top Stage Incubation System, Okolab S.r.l., Pozzuoli, Italy) with temperature and CO₂ control (37 °C, 5% CO₂). An area of 150 × 150 pixels covering 80 × 80 μm² was scanned, collecting photons with a dwell time of 1.2 ms/px. The total acquisition time for one image was 1.7 min. The laser power was ~5 μW and adjusted such that the detector count rate was kept below 5% of the laser pulse frequency to avoid pile-up. For siRNA delivery into the cells via PAMAM dendrimers, the PAMAM dendrimer and the siRNA were mixed in a molar ratio of 2.5:1 (dendrimer : siRNA) and incubated for 30 min to enable complex formation. 6.25 pmol of siRNA were used for transfection. Immediately afterwards, the cells were imaged under the same conditions as with Xfect[®] internalization. Images were taken for 4 h every 15 min, starting immediately after exposure to the siRNA-dendrimer conjugates. Images were generated with SymPhoTime software (PicoQuant); color thresholds of the FLIM images were set based on the lifetime histograms of the full images.

Acknowledgements

Financial support by the Deutsche Forschungsgemeinschaft (Research Training Group GRK 2039/2), the Helmholtz Association (Program MSE) and KIT is gratefully acknowledged. Open access funding enabled and organized by Projekt DEAL.

Conflict of Interest

The authors declare no conflict of interest.

Keywords: cycloaddition · energy transfer · fluorescence · oligonucleotide · transport

- [1] a) J. Soutschek, A. Akinc, B. Bramlage, K. Charisse, R. Constien, M. Donoghue, S. Elbashir, A. Geick, P. Hadwiger, J. Harborth, M. John, V. Kesavan, G. Lavigne, R. K. Pandey, T. Racie, K. G. Rajeev, I. Röhl, I. Toudjarska, G. Wang, S. Wuschko, D. Bumcrot, V. Koteliensky, S. Limmer, M. Manoharan, H.-P. Vornlocher, *Nature* **2004**, *432*, 173–178; b) D. M. Dykxhoorn, J. Lieberman, *Cell* **2006**, *126*, 231–235; c) D. H. Kim, J. J. Rossi, *Nat. Rev. Genet.* **2007**, *8*, 173; d) M. R. Lares, J. J. Rossi, D. L. Ouellet, *Trends Biotechnol.* **2010**, *28*, 570–579.
- [2] a) L. Aagaard, J. J. Rossi, *Adv. Drug Delivery Rev.* **2007**, *59*, 75–86; b) G. Ozcan, B. Ozpolat, R. L. Coleman, A. K. Sood, G. Lopez-Berestein, *Adv. Drug Delivery Rev.* **2015**, *87*, 108–119; c) R. Kanasty, J. R. Dorkin, A. Vegas, D. Anderson, *Nat. Mater.* **2013**, *12*, 967–977.
- [3] K. Wang, J. Huang, X. Yang, X. He, J. Liu, *Analyst* **2013**, *138*, 62–71.
- [4] a) S. Jockusch, A. A. Martí, N. J. Turro, Z. Li, X. Li, J. Ju, N. Stevens, D. L. Akins, *Photochem. Photobiol. Sci.* **2006**, *5*, 493–498; b) A. A. Martí, S. Jockusch, Z. Li, J. Ju, N. J. Turro, *Nucleic Acids Res.* **2006**, *34*, e50–e50.
- [5] a) K. Remdonck, K. Remaut, B. Lucas, N. N. Sanders, J. Demeester, S. C. De Smedt, *Biochemistry* **2006**, *45*, 10614–10623; b) A. Järve, J. Müller, I.-H. Kim, K. Rohr, C. MacLean, G. Fricker, U. Massing, F. Eberle, A. Dalpke, R. Fischer, M. F. Trendelenburg, M. Helm, *Nucleic Acids Res.* **2007**, *35*, e124–e124; c) S. Shin, H.-M. Kwon, K.-S. Yoon, D.-E. Kim, S. S. Hah, *Mol. Biosyst.* **2011**, *7*, 2110–2113; d) M. Hirsch, M. Helm, *Nucleic Acids Res.* **2015**, *43*, 4650–4660.
- [6] a) C. Holzhauser, R. Liebl, A. Goepferich, H.-A. Wagenknecht, M. Breunig, *ACS Chem. Biol.* **2013**, *8*, 890–894; b) C. Holzhauser, H.-A. Wagenknecht, *J. Org. Chem.* **2013**, *78*, 7373–7379; c) J. Steinmeyer, F. Röncke, U. Schepers, H.-A. Wagenknecht, *ChemistryOpen* **2017**, *6*, 514–518; d) J. Steinmeyer, H.-K. Walter, M. A. Bichelberger, V. Schneider, T. Kubar, F. Ronicke, B. Olshausen, K. Nienhaus, G. U. Nienhaus, U. Schepers, M. Elstner, H.-A. Wagenknecht, *Org. Biomol. Chem.* **2018**, *16*, 3726–3731.
- [7] C. Holzhauser, M. M. Rubner, H.-A. Wagenknecht, *Photochem. Photobiol. Sci.* **2013**, *12*, 722–724.
- [8] P. R. Böhländer, H.-A. Wagenknecht, *Eur. J. Org. Chem.* **2014**, 7547–7551.
- [9] R. W. Carthew, E. J. Sontheimer, *Cell* **2009**, *136*, 642–655.
- [10] L. Xu, X. Wang, H. He, J. Zhou, X. Li, H. Ma, Z. Li, Y. Zheng, R. Shao, S. Cen, Y. Wang, *Biochemistry* **2015**, *54*, 1268–1277.
- [11] a) M. Torimura, S. Kurata, K. Yamada, T. Yokomaku, Y. Kamagata, T. Kanagawa, R. Kurane, *Anal. Sci.* **2001**, *17*, 155–160; b) E. M. S. Stennett, M. A. Ciuba, M. Levitus, *Chem. Soc. Rev.* **2014**, *43*, 1057–1075; c) S. Doose, H. Neuweiler, M. Sauer, *ChemPhysChem* **2009**, *10*, 1389–1398; d) T. Heinlein, J.-P. Knemeyer, O. Piester, M. Sauer, *J. Phys. Chem. B* **2003**, *107*, 7957–7964; e) A. Gust, A. Zander, A. Gietl, P. Holzmeister, S. Schulz, B. Lalkens, P. Tinnefeld, D. Grohmann, *Molecules* **2014**, *19*, 15824–15865.
- [12] a) J. Wu, J. Zhou, F. Qu, P. Bao, Y. Zhang, L. Peng, *Chem. Commun.* **2005**, 313–315; b) J. Zhou, J. Wu, N. Hafdi, J.-P. Behr, P. Erbacher, L. Peng, *Chem. Commun.* **2006**, 2362–2364; c) X.-C. Shen, J. Zhou, X. Liu, J. Wu, F. Qu, Z.-L. Zhang, D.-W. Pang, G. Quéléver, C.-C. Zhang, L. Peng, *Org. Biomol. Chem.* **2007**, *5*, 3674–3681; d) X.-x. Liu, P. Rocchi, F.-q. Qu, S.-q. Zheng, Z.-c. Liang, M. Gleave, J. Iovanna, L. Peng, *ChemMedChem* **2009**, *4*, 1302–1310; e) X. Liu, J. Wu, M. Yammine, J. Zhou, P. Posocco, S. Viel, C. Liu, F. Ziarelli, M. Fermeglia, S. Pricl, G. Victorero, C. Nguyen, P. Erbacher, J.-P. Behr, L. Peng, *Bioconjugate Chem.* **2011**, *22*, 2461–2473; f) Y. Cao, X. Liu, L. Peng, *Front. Chem.* **2017**, *11*, 663–675.
- [13] S. Berndl, N. Herzig, P. Kele, D. Lachmann, X. Li, O. S. Wolfbeis, H.-A. Wagenknecht, *Bioconjugate Chem.* **2009**, *20*, 558–564.
- [14] N. N. Dioubankova, A. D. Malakhov, D. A. Stetsenko, M. J. Gait, P. E. Volynsky, R. G. Efremov, V. A. Korshun, *ChemBioChem* **2003**, *4*, 841–847.
- [15] L. Shang, N. Azadfar, F. Stockmar, W. Send, C. Trouillet, M. Bruns, D. Gerthsen, G. U. Nienhaus, *Small* **2011**, *7*, 2614–2620.

Manuscript received: March 30, 2021

Revised manuscript received: June 2, 2021

Accepted manuscript online: June 14, 2021

Version of record online: June 25, 2021